

Tautomerism and Reactivity in Heterocyclic *N*-Oxides. A Spectroscopic and Theoretical Study of Benzimidazole *N*-Oxide Derivatives (*N*-Hydroxybenzimidazoles)

Mariana Boiani,[†] Hugo Cerecetto,^{*,†} Mercedes González,^{*,†} Oscar E. Piro,[‡] and Eduardo E. Castellano[§]

Departamento de Química Orgánica, Facultad de Ciencias-Facultad de Química, Universidad de la República, Iguá 4225, Montevideo 11400, Uruguay, Departamento de Física, Facultad de Ciencias Exactas, Universidad Nacional de La Plata e Instituto IFLP (CONICET), C. C. 67, (1900) La Plata, Argentina, and Instituto de Física de São Carlos, Universidad de São Paulo, C. P. 369, 13560 São Carlos, SP, Brazil

Received: July 16, 2004; In Final Form: October 12, 2004

The tautomeric forms of benzimidazole *N*-oxide derivatives in solution were studied using nuclear magnetic resonance (NMR) techniques. Further insight into the molecular structures was provided by theoretical calculations using density functional theory (DFT). In the gas phase the *N*-hydroxy tautomer was more stable than the *N*-oxide, whereas in solution the stabilization of one form or the other depended on hydrogen bond formation involving the *N*-hydroxy/*N*-oxide moiety. Derivative **4** (*n*-butyl-5-nitrobenzimidazole-2-carboxamide 3-oxide), having a 2-carboxamide moiety, was the only compound studied present as a mixture of tautomers, the *N*-oxide being the predominant one. This was assigned to the formation of an internal hydrogen bond between the *N*-oxide group and the amide hydrogen atom. The tautomeric form present in the solid state was studied for derivative **1** (ethyl-5-nitrobenzimidazole-2-carboxylate 3-oxide) and was conclusively assigned by X-ray diffraction techniques to the *N*-hydroxy tautomer. In the crystal a strong O–H···N intermolecular bond gives rise to supramolecular polymeric chains in the lattice. This strong interaction was also seen in the infrared spectrum and was assigned to two broad bands at 2367 and 2526 cm⁻¹. The vibrational spectrum was satisfactorily described by DFT calculations and an example of this is the prediction of the band corresponding to the N–O stretching (*N*-oxide) just 1% lower than the experimental value. Uncorrelated calculations (HF) were not able to give an unambiguous assignment of this band. The reaction of derivative **1** against different kinds of electrophiles, hard and soft, led only to O-substituted products. This result was explained in terms of the HSAB theory using a local–global approach.

Introduction

Benzimidazole *N*-oxides present a very interesting chemistry, and a number of reviews covering its synthesis and reactivity can be found.^{1–3} At difference with other heterocyclic *N*-oxides, they are not obtained by direct *N*-oxidation of benzimidazoles,^{2,4} a fact that has led to the development of an extensive and rich chemistry around this system. Besides, benzimidazole *N*-oxide derivatives unsubstituted at nitrogen-1 (N-1) present a tautomeric equilibrium with the corresponding *N*-hydroxy form (Figure 1). Although, conventionally, these benzimidazoles are described as *N*-oxide derivatives, account must be taken of the corresponding *N*-hydroxybenzimidazole tautomer. Previous studies⁵ on the parent compound (benzimidazole-3-oxide), using UV spectroscopy, have shown that while *N*-hydroxy tautomer is the main form in apolar solvents (cyclohexane) the equilibrium is shifted to the *N*-oxide as polarity or hydrogen-bonding power increase. In aqueous solution benzimidazole 3-oxide is predominantly in the *N*-oxide form. A similar behavior was shown for 5-nitrobenzimidazole 3-oxide by inspection of its UV spectrum in water and ethanol. The 2-phenylbenzimidazole 3-oxide, however, appears to exist predominantly in the *N*-

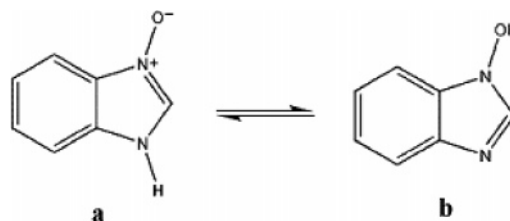


Figure 1. Tautomeric equilibrium in benzimidazole *N*-oxide.

hydroxy form even in polar solvents.⁶ NMR spectroscopy, a technique widely used in the study of tautomeric equilibria for a number of different chemical systems, has not been used on benzimidazole *N*-oxide studies, and information on ¹³C NMR data is extremely scanty. Regarding the position of the equilibrium in the solid state no conclusive evidence is available.

Benzimidazole *N*-oxide unsubstituted at nitrogen has two nucleophilic centers (N, O), which could lead to two substitution products (N-substituted, O-substituted) in an electrophilic attack. This situation can be further complicated by the presence of two tautomeric forms. It is clear that in the study of the chemistry of this system both forms have to be considered in order to explain the reactivity observed. Although no systematic study on the reaction of these derivatives with electrophiles has been conducted an important amount of information is available.² Interestingly, reaction of benzimidazole *N*-oxide derivatives with various alkylating/acylating agents leads to the corresponding *N*-alkoxy/*N*-acyloxy benzimidazoles, and no

* To whom correspondence should be addressed. E-mail: (H.C.) hcerecet@fq.edu.uy; (M.G.) megonzal@fq.edu.uy. Telephone: (5982) 525-8618/216. Fax: (5982) 525-0749.

[†] Universidad de la República.

[‡] Universidad Nacional de La Plata e Instituto IFLP (CONICET).

[§] Universidad de São Paulo.

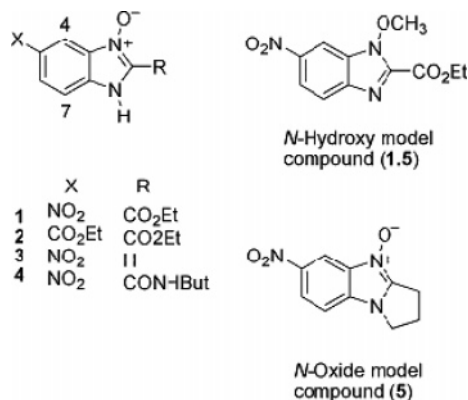


Figure 2. Structures of benzimidazole *N*-oxide derivatives used in the tautomeric study in solution. Atom nomenclature employed for NMR assignments is indicated.

TABLE 1: Experimental and Calculated ¹H and ¹³C Chemical Shifts of Derivative 1 and of Model Compounds 1.5 and 5

| | ¹ H δ (ppm) | | ¹³ C δ (ppm) | |
|--------------------------------|------------------------|------|-------------------------|--------|
| | 4 | 7 | 4 | 7 |
| CDCl ₃ | 8.62 | 7.96 | 108.02 | 123.10 |
| acetone- <i>d</i> ₆ | 8.52 | 7.96 | 107.03 | 122.34 |
| DMSO- <i>d</i> ₆ | 8.42 | 7.98 | 108.10 | 122.90 |
| MeOD | 8.56 | 7.92 | 107.46 | 121.50 |
| D ₂ O | 8.64 | 7.79 | a | a |
| 6-31G*(1b) | 9.31 | 8.20 | 111.61 | 121.24 |
| 6-31G*(1a) | 10.04 | 7.40 | 123.57 | 106.00 |
| 1.5 ^b | 8.52 | 7.97 | 107.10 | 123.31 |
| 6-31G* | 9.22 | 8.12 | 109.30 | 119.15 |
| 5 ^c | 8.58 | 7.75 | 110.60 | 112.40 |
| 6-31G* | 9.82 | 7.32 | 120.84 | 105.20 |

^a Because of solubility problems it was not possible to obtain carbon data. ^b CDCl₃. ^c Acetone-*d*₆.

conclusive evidence on obtaining the *N*-substituted products has been presented.

The chemistry of heterocyclic amine *N*-oxides has raised widespread interest due to the exceptionally high bioactivity of these compounds.^{7,8} Despite little being known regarding the biological spectrum of the benzimidazole *N*-oxide system, various derivatives have been described as antihelmintic,⁹ acaricides, antibacterial,¹⁰ and trypanocidal agents.¹¹ What is more, 1-hydroxybenzimidazole derivatives have shown central depressant effects¹² and *N*-alkoxybenzimidazoles has been described as anti-HIV agents.^{13,14} These compounds have also found application in the field of organic chemistry as synthetic intermediates.¹⁵ Both for the study of its biological activity and for its synthetic applications, it is necessary to obtain insight into the tautomeric equilibrium and its chemical consequences.

In light of the preceding considerations, the present work was undertaken to study the tautomerism of benzimidazole *N*-oxide derivatives in solution and in the solid state. Experimental support for the existence of the corresponding tautomers was obtained from nuclear magnetic resonance (NMR), infrared (FTIR), and X-ray diffraction (X-ray) techniques, along with theoretical calculations using the density functional theory (DFT) approach. Finally, the reactivity of these derivatives against electrophiles was rationalized in terms of Pearson's hard and soft acid base (HSAB) theory.

Experimental Section

Synthesis. Compounds **1–4** (Figure 2) and **1.1–1.8** (Table 5) were obtained as described in the literature.¹¹ Spectroscopic characterization of new compounds (**1.2**, **1.6–1.8**) is given as

Supporting Information. Compound **5** was obtained as previously reported.¹⁶

NMR spectra were acquired with a Bruker DPX-400 spectrometer equipment at 303 K, using the standard sequences and samples were dissolved in different deuterated solvents (DMSO-*d*₆, CDCl₃, MeOD, acetone-*d*₆, D₂O). TMS (tetramethylsilane) was used as an internal reference. FTIR spectra were recorded with a resolution of 4 cm⁻¹, on a Perkin-Elmer 1310 apparatus, using KBr wafers containing 1% of the sample.

Diffraction Data. The crystal and molecular structure of derivative **1** (Ethyl 5-nitrobenzimidazole-2-carboxylate 3-oxide) has been determined by X-ray diffraction methods. The diffraction pattern was collected at 120 K on an Enraf-Nonius KappaCCD diffractometer employing graphite monochromate Mo K α radiation and φ and ω scans to explore the reciprocal space. Data were collected with the program COLLECT¹⁷ and reduced with DENZO and SCALEPACK.¹⁸ The compound crystallizes in the monoclinic *P*2₁/*n* space group with *a* = 4.4840(3) Å, *b* = 10.188(1) Å, *c* = 23.106(2) Å, β = 91.008(3)°, and *Z* = 4. The structure was solved by direct¹⁹ and Fourier²⁰ methods from 1253 reflections with *I* > 2 σ (*I*) and refined by full-matrix least-squares²⁰ procedure to an agreement R1-factor of 0.052. All but the hydroxyl and the methyl H atoms were positioned stereochemically and refined with the riding model. The hydroxyl and methyl hydrogen atoms were refined as rigid groups and allowed to rotate around the corresponding N–O and C–C bonds, respectively. As expected, the CH₃ refined positions converged to a staggered methyl configuration. Listings of atomic coordinates and equivalent isotropic displacement parameters, full intramolecular bond distances and angles, hydrogen coordinates and anisotropic displacement parameters were deposited in the Cambridge Crystallographic Data Centre, reference number CCDC-242406.

Computational Methods. Calculations were performed with the Spartan'04, 1.0.1 version, suite of programs.²¹ Molecules were constructed using standard geometries and bond lengths. The initial conformations were obtained from a systematic search using molecular mechanics force field (MMFF).²² Both tautomeric structures were fully optimized using the gradient-corrected density functional methodology: Becke's exchange functional (B)²³ and Becke's three-parameter adiabatic connection (B3) hybrid²⁴ exchange functional were used in combination with the Lee–Yang–Parr correlation functional.²⁵ The standard 6-31G* basis set of DZP quality was used for orbital expansion to solve the Kohn–Sham equations for first and second-row elements. For heavier atoms a pseudopotential base (LACVP*)²⁶ was used. Subsequently, the harmonic vibrational frequencies and IR intensities were calculated at the same level of theory.

Polarizable continuum model (PCM)^{27,28} calculations were carried out with GAMESS for windows.^{29,30}

¹H and ¹³C magnetic shielding tensors of HF-optimized (6-31G*) structures were obtained following the gauge-including atomic orbital (GIAO) approach at the same level.^{31–33} To compare isotropic shieldings with the experimentally observed chemical shifts, the NMR parameters for TMS (tetramethylsilane) were calculated and used as the reference molecule.

Results and Discussion

Tautomeric Equilibrium in Solution. There are many examples in the literature of studies of tautomeric equilibria by NMR spectroscopy.³⁴ Since it is virtually impossible to obtain separate NMR spectral patterns for both tautomers, quantitative estimates of tautomeric composition have to be based on the average NMR shielding referred to those of suitable model

TABLE 2: Experimental and Calculated ^1H and ^{13}C Chemical Shifts of Derivatives 2–4

| | | ^1H δ (ppm) | | ^{13}C δ (ppm) | |
|----------------------|--------------------------------|-----------------------------|-------------|--------------------------------|-----------------|
| | | 4 | 7 | 4 | 7 |
| 2 | CDCl_3 | 8.38 | 7.86 | 113.17 | 122.04 |
| | 6-31G* 2b (2a) | 8.79 (9.59) | 8.14 (7.28) | 115.23 (127.63) | 121.09 (105.41) |
| 3^a | $\text{DMSO}-d_6$ | 8.37 | 7.84 | 106.89 | 121.24 |
| | 6-31G* 3b (3a) | 9.05 (9.95) | 8.11 (7.36) | 108.55 (121.82) | 119.70 (105.99) |
| 4^b | $\text{DMSO}-d_6$ | 8.37 (8.58) | 7.93 (7.72) | 110.23 (117.10) | 124.21 (114.09) |
| | CDCl_3 | 8.57(8.74) | 7.94 (7.68) | 108.81 (117.87) | 121.21 (112.86) |
| | 6-31G* 4b (4a) | 9.31 (9.93) | 8.05 (7.50) | 112.13 (121.56) | 119.39 (107.02) |

^a Insoluble in chloroform. ^b Present as a tautomeric mixture, in parentheses are indicated chemical shifts of the *N*-oxide tautomer.

TABLE 3: Relative Energies^a (E_{rel} , kcal/mol) for Tautomers **1a and **4a****

| method | 1a E_{rel} | 4a E_{rel} |
|--|----------------------------|----------------------------|
| B3LYP/6-31G* | 6.5 | 3.6 |
| B3LYP/6-31G** | 7.7 | 4.8 |
| B3LYP/6-31+G* | 5.0 | 2.2 |
| PCM/B3LYP/6-31+G* (H_2O) | -0.5 | -1.4 |
| PCM/B3LYP/6-31+G* (CHCl_3) | 2.9 | 0.5 |

^a The energy of the corresponding *N*-hydroxy tautomer is taken as zero.

TABLE 4: Comparison of Selected Molecular Coordinates for X-ray Structure and Optimized DFT Geometry of **1^a**

| | X-ray | B3LYP/6-31G* | |
|----------------------|-------|----------------|-----------|
| | | 1b | 1a |
| O(1)–N(1) | 1.374 | 1.377 (+0.22) | 1.267 |
| N(1)–C(2) | 1.358 | 1.378 (+1.47) | 1.356 |
| N(1)–C(3) | 1.376 | 1.365 (–0.80) | 1.413 |
| N(2)–C(2) | 1.330 | 1.326 (–0.30) | 1.385 |
| N(2)–C(8) | 1.375 | 1.369 (–0.44) | 1.363 |
| C(2)–N(1)–O(1) | 127.1 | 128.5 (+1.4) | 129.2 |
| N(2)–C(2)–N(1) | 111.9 | 112.5 (+0.6) | 109.4 |
| N(2)–C(2)–C(1)–O(22) | –19.2 | 180.0 (–160.8) | 0.2 |

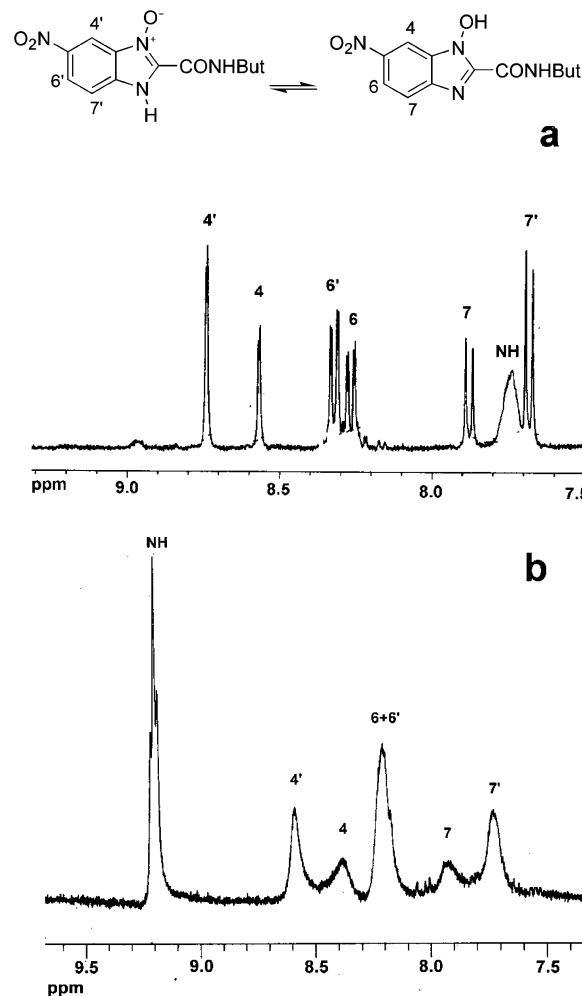
^a Numbering according to the ORTEP drawing. Bond lengths are in angstroms and angles in degrees. In parentheses: deviation of DFT values from X-ray values in percentage for bond length and in degrees for angles.

compounds. Model compounds are usually the corresponding *N*-methyl and *O*-methyl derivatives. Herein, the tautomeric equilibrium of ethyl 5-nitrobenzimidazole-2-carboxylate 3-oxide (**1**) was studied in solution using model compounds (**1.5** and **5**) (Figure 2). To assess the effect on tautomeric equilibrium of different substituents at 2- and 5-aromatic positions, derivatives **2–4** were used (Figure 2).

It is difficult to assign the tautomeric form from proton chemical shift solely because differences in chemical shifts are very small ($|\Delta\delta| = 0.06$ and 0.22 ppm for H-4 and H-7, respectively, between model compounds; see Table 1). Besides, the vicinity of the *N*-oxide/*N*-hydroxy moieties acts to increase solvent effects through hydrogen bonding and/or polar interactions.

On the other hand, carbon signals allowed for a clear assignment of the tautomeric structure. By a comparison of the two model compounds it can be seen that while carbon 4 is similarly shielded in both “tautomers” ($|\Delta\delta| = 3.50$ ppm), carbon 7 is more shielded under the *N*-oxide form ($|\Delta\delta| = 10.91$ ppm). The shielding effect of the *N*-oxide form is due to the amine character of the adjacent nitrogen (N-1). Under the *N*-hydroxy form this same nitrogen has an imine character. A similar trend was reported for benzotriazole 1-oxide and 1-hydroxybenzotriazole tautomers.³⁵

Since NMR experiments are carried out in diluted solutions (≈ 0.1 M) intramolecular as well as solute–solvent interactions

**Figure 3.** ^1H NMR spectra of derivative **4** showing aromatic signals corresponding to both tautomers: (a) CDCl_3 ; (b) $\text{DMSO}-d_6$.

are expected to prime. In DMSO and acetone (polar, hydrogen-bond-acceptor, HBA) solutions derivative **1** is present as **1b**, which could be attributed to the formation of a hydrogen bond between the hydroxyl moiety and the solvent. In methanol, a polar solvent that could act as a hydrogen-bond-donor (HBD) as well as acceptor, both tautomeric forms can be stabilized by hydrogen bonding with the solvent but only the *N*-hydroxy form is evidenced by NMR. Since 5-nitrobenzimidazole *N*-oxide is more acid ($\text{p}K_a = 6.1$)² than methanol ($\text{p}K_a = 16.6$)³⁶ it is expected to act as the HBD through the hydroxyl moiety, thus stabilizing **1b**. In chloroform (less polar and weak HBD) solution compound **1** is also present as the *N*-hydroxy tautomer, which could be explained by the formation of an internal hydrogen bond between the hydroxyl moiety and the 2-carboxyl group. Although in water solution it was not possible to obtain a ^{13}C NMR spectrum, proton chemical shifts (H-7 = 7.79 ppm

TABLE 5: Experimental and DFT-Calculated Frequencies (cm⁻¹) for Derivative 1 and Model Compounds 1.5 and 5

| | exptl band ^a | | | <i>N</i> -hydroxy (DFT) ^c | | | <i>N</i> -oxide (DFT) ^c | | |
|------------|-------------------------|--------------------|------------------|--------------------------------------|------------------|------------------|------------------------------------|------------------|------------------|
| | $\nu(\text{NH/OH})$ | $\nu(\text{NO})^b$ | $\nu(\text{CO})$ | $\nu(\text{OH})$ | $\nu(\text{NO})$ | $\nu(\text{CO})$ | $\nu(\text{NH})$ | $\nu(\text{NO})$ | $\nu(\text{CO})$ |
| 1 | 2367, 2526 | 1223 | 1728 | 3334 | 1157 | 1748 | 3642 | 1263 | 1757 |
| 1.5 | | 1221 | 1728 | | 1155 | 1793 | | | |
| 5 | | 1258 | | | | | | 1244 | |

^a KBr. ^b Tentative assignment (see text). ^c B3LYP/6-31G*, frequencies are unscaled.

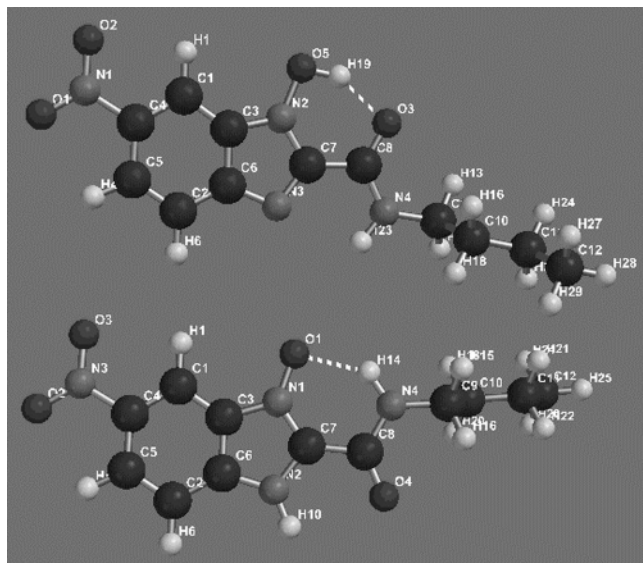


Figure 4. Optimized geometry (B3LYP/6-31G*) of tautomeric species of derivative **4**, showing intramolecular hydrogen bond formation: (**4a**) $d(\text{O1}\cdots\text{H14}) = 1.948 \text{ \AA}$, $d(\text{O1}\cdots\text{N4}) = 2.795 \text{ \AA}$, $\angle(\text{O1-H14-N4}) = 138.1^\circ$; (**4b**) $d(\text{O3}\cdots\text{H19}) = 1.734 \text{ \AA}$, $d(\text{O5}\cdots\text{O3}) = 2.639 \text{ \AA}$, $\angle(\text{O5-H19-O3}) = 148.1^\circ$.

compared to 7.75 ppm for **5** and 7.97 for **1.5**) point to the presence of the *N*-oxide form, in agreement with previous findings using UV spectroscopy.⁵

Different substituents at the 5-aromatic position seem to have no relevant effect on the tautomeric equilibrium, derivatives **1–2** (and benzimidazole-3-oxide)⁵ were present as *N*-hydroxybenzimidazoles in the solvents studied (Table 2). On the other hand, a change in the 2-aromatic position could have a pronounced effect on tautomeric equilibrium. Compound **3**, 2-unsubstituted, is present as the *N*-hydroxybenzimidazole in DMSO solution, confirming previous UV spectroscopy studies.⁵ However, the 2-carboxamide derivative **4** is present as a mixture of tautomers in DMSO and chloroform solution (Table 2, Figure 3). In this derivative another hydrogen bond is possible between the *N*-oxide moiety and the amide hydrogen of the 2-carboxamide group (Figure 4). A rough estimation of the proportion of the two tautomers was obtained by integrating the experimental proton signals, showing 44% and 38% for **4b** and 56% and 62% for **4a** in chloroform and DMSO solution, respectively, at 303 K. This is in agreement with previous studies involving the prototropic equilibrium of the *N*-oxide function, which concluded that acidic solvents stabilize the *N*-oxide form by protonation of the NO oxygen atom.³⁷ In the present case an internal HBD moiety could act as the acid.

Aromatic proton signals for derivative **4** in DMSO solution are broad due to faster tautomeric equilibrium than in CDCl₃ solution at 303 K. Acquisition of ¹H NMR data at higher temperature ($T = 313\text{--}343 \text{ K}$, Figure 1S) showed that signals coalescence near 333 K. However, tautomeric composition was unaffected. Similar results were seen with derivative **1** where

only signals corresponding to **1b** were evidenced in ¹H NMR spectrum at different temperatures ($T = 238\text{--}343 \text{ K}$, Figure 2S).

Using the utilities available in the Spartan'04 suite of programs the HF/6-31G*-simulated NMR spectra of derivatives **1–4** and model compounds were obtained in the gas-phase (Tables 1 and 2). Calculated proton chemical shifts for the *N*-hydroxy form agree very well with experimental values with an average error of 8% and 3% for H4 and H7, respectively. Carbon chemical shifts of C4 and C7 have an even smaller average error (2%). While chemical shifts for the *N*-oxide tautomer display a higher average error (H4 = 14%, H7 = 4%, C4 = 6%, C7 = 5%), results are in good agreement with experimental data. These results are encouraging, since they allowed the use of a medium basis set to study spectroscopic properties of *N*-oxide containing compounds with a low error.

The study of tautomeric equilibrium in the gas phase of derivatives **1** and **4** was performed using density functional theory (DFT) with the B3LYP functional (Table 3). This methodology has been proved to be useful to describe tautomeric equilibria.^{38,39} Since there is the possibility of an internal hydrogen bond, the effect of polarization functions on hydrogen atoms as well as the effect of diffuse functions on heavy atoms was analyzed. The results indicate that for both derivatives the most stable tautomer in the gas phase is the *N*-hydroxy. However, the energy difference for derivative **4** is lower. This could be attributed to the stabilization of the *N*-oxide form by an internal hydrogen bond with the 2-carboxamide moiety. As expected the energy profile is better described when diffuse functions are included. Solvent effects were also analyzed using a polarized continuum model (PCM) in water and chloroform (Table 3). Once a solvent such as chloroform is included the energy difference in favor of the *N*-hydroxy tautomer is reduced. The small difference obtained for the 2-carboxamide derivative is in perfect agreement with NMR studies where the coexistence of both forms in chloroform solution is evidenced. In water solution, as expected, the *N*-oxide form is the most stable one for both derivatives.

Tautomeric Equilibrium in the Solid State. As mentioned before, almost nothing is known regarding the position of the equilibrium in the solid state.² To gain insight into the tautomeric forms present in the solid, X-ray crystallography and infrared spectroscopy were used.

In Figure 5, an ORTEP⁴⁰ drawing of derivative **1** is shown. The nitro group and the heterocycle system are coplanar to within experimental accuracy (rms deviation of atoms from the least squares plane of 0.026 Å) and the ester moiety is tilted from this plane by 22.1(3)°. This structure differs from the optimized geometry in the gas phase (DFT). Whereas the dihedral angle between the ester moiety and the *N*-hydroxy moiety is 0.0° in DFT-optimized geometry due to an intramolecular hydrogen bond, only intermolecular hydrogen bonds are formed in the crystal. Selected geometric parameters from the X-ray structure and DFT optimized geometry of **1** are compared in Table 4, along with the values for the *N*-oxide form of **1** at the same level of theory. DFT methodology gives a lower

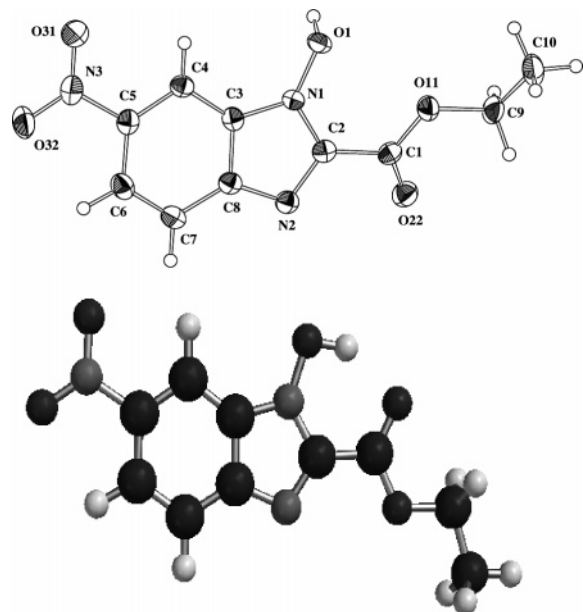


Figure 5. Molecular plot of derivative **1** showing the labeling of the non-hydrogen atoms and their displacement ellipsoids at the 50% probability level (up), and the DFT (B3LYP/6-31G*) optimized geometry of **1b** in the gas phase (down).

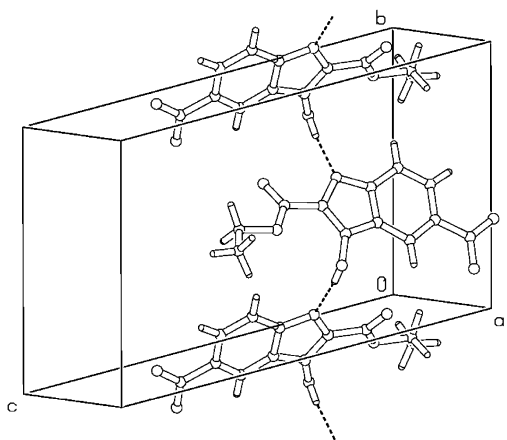


Figure 6. Crystal packing drawing of **1** displaying the polymeric structure generated by the O–H...N intermolecular bonding in the solid ($d(\text{O1}\cdots\text{N2}') = 2.673 \text{ \AA}$, $d(\text{H1}\cdots\text{N2}') = 1.837 \text{ \AA}$, $\angle(\text{O1-H1}\cdots\text{N2}') = 173.9^\circ$). Neighboring molecules on the polymer are related to each other through a crystallographic screw-axis parallel to the unit cell *b*-axis.

average error in bond lengths (0.65%) as compared to HF using the same basis set (1.34%) (Table 1S). However, while HF yields always shorter bonds, DFT results are varied.

The crystal is stabilized by a strong and linear intermolecular hydrogen bond (O1–H1...N2'), involving the *N*-hydroxy group and the heterocycle nitrogen atom of a neighboring, 2-fold-screw-axis symmetry related, molecule. This interaction gives rise to supramolecular helices parallel to the crystallographic unique axis, as shown in the PLUTON⁴¹ drawing of Figure 6. X-ray diffraction data conclusively confirm the tautomeric structure of **1** in the solid state as *N*-hydroxybenzimidazole.

The infrared spectrum of derivative **1** is depicted in Figure 7. The bands at 3110 and 2980 cm^{-1} belong to $\nu(\text{C-H})$ vibrations.⁴² Two broad bands at 2367 and 2526 cm^{-1} can be attributed to the $\nu(\text{N}\cdots\text{H-O})$ interaction,⁴³ in agreement with crystallographic data. The strong band at 1728 cm^{-1} is attributed to the $\nu(\text{C=O})$ vibration of the ester function.⁴² Finally, two bands at 1528 and 1346 cm^{-1} are assigned to the $\nu(\text{N-O})$ stretching of the nitro moiety.

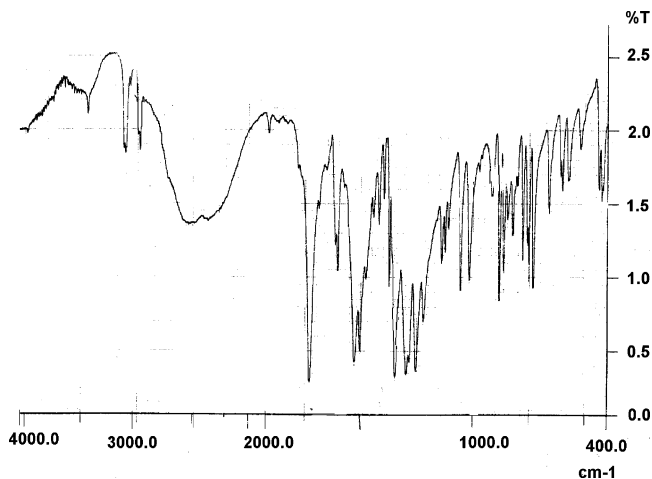


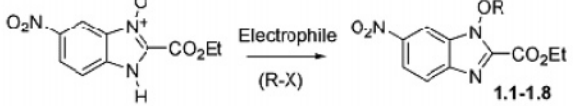
Figure 7. Experimental FTIR spectrum of the solid **1** sample.

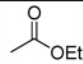
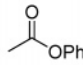
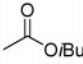
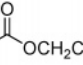
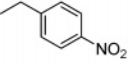
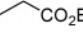
Any unambiguous assignment of the N–O stretch was precluded by the preponderance of bands between 1300 and 1200 cm^{-1} . By inspection of the spectrum, a tentative assignment was made ($\nu(\text{N-O})$ 1223 cm^{-1}). This is quite in agreement with previous data on benzimidazole *N*-oxide derivatives (1249 cm^{-1}).⁴⁴

In Table 5 are presented experimental and calculated (DFT) infrared bands for **1** and model compounds **1.5** and **5**. Despite that calculated geometric parameters fit those obtained by X-ray diffraction fairly well, the conformation in the gas phase is quite different. This makes direct comparison of calculated and experimental IR bands not straightforward. Since errors in geometric parameters were varied no scaling factor was used for calculated frequencies. The bands between 2300 and 2500 cm^{-1} , present in the solid sample, are not seen in the DFT-calculated IR spectrum as they arise from intermolecular interactions. In general, calculated infrared bands from both tautomeric species point to good agreement with the experimental data. DFT methodology showed an overall better performance than the HF/6-31G* calculation. The unambiguous attribution of calculated frequencies in the latter case was much more difficult. While 6-31G* yielded a value of 1250 cm^{-1} for the N–O stretching (*N*-hydroxy), close to the experimental value (2% higher), the value obtained for the *N*-oxide tautomer is presumed to be overestimated (1365 cm^{-1} for **1**, 6-31G* did not provide an unambiguously attributable N–O stretching for compound **5**). An example of the potential of the DFT calculations is the prediction of the band corresponding to the N–O stretching for compound **5** (*N*-oxide) at 1244 cm^{-1} , just 1% lower than the experimental value (Table 5).

Derivative **4** was the only benzimidazole *N*-oxide derivative studied that was present as a tautomeric mixture in solution. Since it was not possible to obtain a suitable crystal for X-ray diffraction studies, its tautomeric form in the solid was analyzed by IR spectroscopy (Figure 3S). The infrared spectrum of this derivative showed a weak band at 3393 cm^{-1} assigned to $\nu(\text{N-H})$ stretching of the amide moiety and a weak broad band at 3166 cm^{-1} corresponding to the $\nu(\text{N-H})$ stretching of an associated form. The band at 1273 cm^{-1} was assigned to the N–O stretching of the *N*-oxide moiety. From these data it can be suggested that derivative **4** is present in the solid state under the *N*-oxide form. A simulated IR spectrum using DFT methodology was in agreement with the experimental one (data not shown).

Reactivity of Benzimidazole *N*-Oxide toward Electrophiles. To explain, on a theoretical ground, the regiochemistry

TABLE 6: Reaction of 1 with Different Electrophiles


| | Electrophile ^a | R | Base / Time | Yield % ^{b,c} | |
|------|-------------------------------|---|--|------------------------|------------|
| Hard | Ethyl chloroformate |  | None / 30 min | 30 | 1.1 |
| | Phenyl chloroformate |  | None / 50 min | 41 | 1.2 |
| | <i>i</i> Butyl chloroformate |  | None / 60 min | 74 | 1.3 |
| | Trichloroethyl chloroformate |  | None / 10 min | 76 | 1.4 |
| Soft | Methyl iodide | CH ₃ | NaHCO ₃ / 7 days ^d | 100 | 1.5 |
| | Pentyl iodide | (CH ₂) ₄ CH ₃ | NaHCO ₃ / 6 days ^d | 61 | 1.6 |
| | <i>p</i> -Nitrobenzyl bromide |  | NaHCO ₃ / 6 days ^d | 43 | 1.7 |
| | Ethyl bromoacetate |  | NaHCO ₃ / 3 days ^d | 40 | 1.8 |

^a Stoichiometry 1:1. ^b Chromatographic isolated compounds, yields were not optimized. ^c Only O-substituted products and unreacted 1 were evident in the reaction media. ^d 2 equiv of base per equivalent of 1.

observed, the reaction between **1** and a set of electrophiles was assayed in acetone at room temperature. The reaction was followed by thin-layer chromatography and was stopped when an important consumption of the starting material was evidenced. In every case, the reaction led only to one product and some starting material could be recovered in the purification processes. While conditions employed (time, use of base) were different, hard as well as soft electrophiles yielded exclusively O-substituted products (Table 6). The substitution site was confirmed by ¹³C NMR and NOEdiff experiments (Figure 4S). This result was analyzed in terms of Pearson HSAB (hard and soft acid base) theory at a DFT level (B3LYP/6-31G*).

In the context of the hard and soft acids and bases principle (HSAB) reactivity of molecules is related to properties of the system such as hardness (η) and electronegativity (χ).⁴⁵ The hardness (η) is the change of chemical potential (μ) with respect to the number of electrons (N) and represents the resistance of the chemical potential to change in the number of electrons. In eq 1, E stands for the energy of the system and V is the external potential.

$$\eta = (\delta\mu/\delta N) = (\delta^2 E/\delta N^2)v \quad (1)$$

The electronegativity (χ) is the negative of the chemical potential (μ) and is the power of the system to attract electrons to it.

$$\chi = -(\delta E/\delta N)v = -\mu \quad (2)$$

For the reaction of A and B the fractional number of electrons transferred (ΔN) can be written as follows

$$\Delta N = \chi_A - \chi_B/2(\eta_A + \eta_B) \quad (3)$$

From this equation it can be concluded that the difference in electronegativities is the driving force of the reaction, while the sum of the hardness parameters inhibits electron transfer.⁴⁵

TABLE 7: Global Hardness (η_{DFT}) and Electronegativity (χ_{DFT}) Values for **1 and Two Electrophiles**

| | η_{DFT} (eV) | χ_{DFT} (eV) |
|---------------------|--------------------------|--------------------------|
| 1b | 1.98 | 4.68 |
| 1a | 1.68 | 4.32 |
| ethyl chloroformate | 4.04 | 4.19 |
| methyl iodide | 3.05 | 3.94 |

Electronegativity and hardness can be easily obtained using Koopman's approximation, from the energy values of frontier orbitals (ϵ_{H} , ϵ_{L}).⁴⁶

$$\eta = (\epsilon_{\text{L}} - \epsilon_{\text{H}})/2 \quad (4)$$

$$\chi = -(\epsilon_{\text{L}} + \epsilon_{\text{H}})/2 \quad (5)$$

In an HSAB global approach, global hardness (η) and electronegativity (χ) for **1** and two electrophiles (one hard and one soft) were determined (Table 7). To assess the accuracy of the method employed, DFT-calculated and experimental values of η a χ for a number of compounds described in the literature were compared (Table 2S, Figure 5S).⁴⁵ DFT-calculated electronegativities were lower than experimental ones and were linearly related in the range of values studied ($\chi_{\text{DFT}} = 1.7-6.2$ eV, $\chi_{\text{exp}} = 1.5-7.2$ eV). The DFT-calculated hardness parameter, however, presented a very small range of linearity ($\eta_{\text{DFT}} = 3.0-4.8$ eV), and errors were more erratic. Similar results were obtained when a HF/6-31G* methodology was employed (Figure 6S). Since both tautomeric forms of **1** have a η_{DFT} value outside this range it would be unadvisable to draw any conclusion from it. In consequence, the fractional number of electrons transferred (ΔN) was not calculated. Regarding electronegativities values for both, electrophiles and nucleophiles, were statistically equal (Figure 5S).

The fact that **1** reacts with different kinds of electrophiles, hard and soft, could imply that HSAB theory is not working in

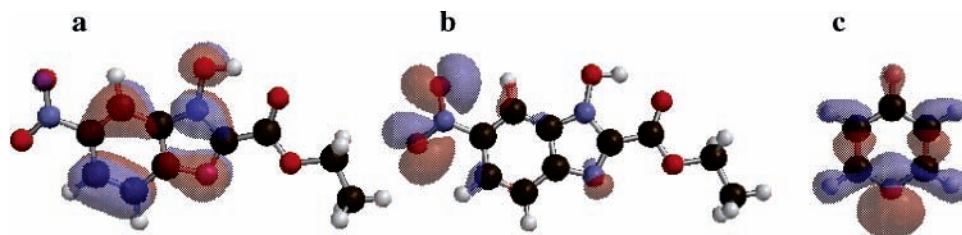


Figure 8. Molecular orbitals involved in nucleophilic attack: (a) HOMO of **1**; (b) HOMO-2 of **1**; (c) HOMO of pyridine.

TABLE 8: Fukui Function (f^-) and EP Charges^a for Compound **1**

| | 1b | 1a |
|-----------------|-----------|-----------|
| $f^-(\text{O})$ | 0.3626 | 0.8788 |
| EP(O) | -0.429 | -0.451 |
| $f^-(\text{N})$ | 0.3004 | 0.3208 |
| EP(N) | -0.548 | -0.388 |

^a All quantities are expressed in atomic units.

a global–global level but in a local–global level. While chemical potential is a global property, and is constant everywhere within the molecule, hardness is a function of position. Using density functional theory the reactive sites in a molecule can be determined by the Fukui functions, f .⁴⁶ There are three different Fukui functions, f^- , f^+ , and f^0 , depending on whether the molecule is acting as a nucleophile, an electrophile or as both. In the frozen core approximation, the Fukui functions are expressed in terms of the frontier orbital density. In the case of a nucleophilic attack the Fukui function (f^-) is approximated to the normalized electron density of the HOMO as shown in eq 6.

$$f^-(k) = c_{\alpha,k}(\text{HOMO})^2 + c_{\beta,k}(\text{HOMO})^2 \quad (6)$$

From the Li–Evans⁴⁷ reactivity and selectivity rules, for soft–soft interactions, the preferred reactive site in a molecule would have the highest value of f , whereas the preferred site for hard–hard interactions would be described through the minimum value of f . While this criterion works well with molecules with only one reactive site,^{48–51} problems have been encountered when working with polyfunctional systems.⁵² In these systems, Fukui functions give a good description of soft–soft interactions but sometimes fail to describe hard–hard interactions. Since hard–hard interactions are charge-controlled, charges have been proposed as better descriptors. In the present case, a condensed Fukui function (f^-) and electrostatic-fit charges (EP) for both nucleophilic centers were determined at the same level of theory for derivative **1** (Table 8).

By inspection of Table 8, a number of conclusions could be drawn. First, under the *N*-oxide form the oxygen atom is, clearly, a soft nucleophile (larger f^-), as can be expected from its anion character.⁴⁵ Surprisingly, the oxygen atom could be also considered a hard nucleophile from its larger negative charge. As has been stated before, hard–hard interactions are driven by electrostatic forces and the site of electrophilic attack would be that of larger negative charge, which may or may not coincide with a small value of f . Therefore, under the *N*-oxide form, the oxygen atom is the preferred site of electrophilic attack for both, hard and soft, electrophiles. This is in perfect agreement with the distribution of products observed.

Second, under the *N*-hydroxy form the oxygen atom is again softer than the nitrogen, but the nitrogen atom is more negatively charged. On the basis of only this result, it could be concluded that the nitrogen atom should be the most susceptible site to electrophilic attack by a hard electrophile, going against the

experimental evidence. Since DFT calculations are in the gas-phase it can be argued that the conformation in solution would differ, leading to a different electronic distribution. This possibility was analyzed by studying the variation of EP charges as a function of conformation (Figure 7S), but an identical trend was obtained. Theoretical results seem to make chemical sense, since being N-1 a pyridine type nitrogen (under the *N*-hydroxy form) it would be expected to react with acylating agents in the same way as pyridine does. However, if the molecular orbitals (HOMO) for **1** and pyridine are compared clear differences appear (Figure 8a and 8c). The HOMO orbital of **1** has no contribution from the electron lone pair of the nitrogen atom. This pair of electrons is situated in a lower energy orbital, HOMO-2 (Figure 8b).

Conclusions

From the data herein presented, it may be concluded that the *N*-hydroxy tautomer is intrinsically more stable than the *N*-oxide in the gas phase. The stabilization of one form or the other in solution will depend on interactions of the *N*-hydroxy/*N*-oxide moiety via hydrogen bond formation either intramolecular or with the solvent. Thus, HBA solvents, such as DMSO and acetone, would stabilize the *N*-hydroxy tautomer, while HBD solvents would stabilize the *N*-oxide one. In solvents that can act as both, HBD–HBA, the stabilization of one form or the other would depend on acid–base properties. However, substituents with hydrogen-bond donor (HBD) capability at 2-aromatic position would help stabilize the *N*-oxide species even in HBA solvents. In less polar solvents, such as chloroform, the predominance of one tautomer will depend mainly on intramolecular interactions. Remarkably, different substituents at aromatic positions as well as different solvents have a small effect on carbon 7 chemical shifts, which makes ¹³C NMR a powerful technique for the study of this equilibrium. Besides, the HF-calculated NMR spectrum is consistent with the experimental results.

The X-ray diffraction experiment allowed for the conclusive identification of the *N*-hydroxy tautomer as the one present in the solid state. This result was also in agreement with the bands present in the IR spectrum. Density functional theory (DFT) calculations aimed at describing the vibrational structure of the two tautomeric species fit fairly well with the experimental data. Besides, DFT methodology was able to predict the N–O stretching (*N*-oxide moiety) accurately, while uncorrelated calculations (6-31G*) could not give an unambiguous assignment of this band.

Reaction of benzimidazole *N*-oxide **1** with different electrophiles, hard and soft, led only to O-substituted products. These results were explained using local HSAB descriptors (f , EP) at a DFT level. Under the *N*-oxide form the oxygen atom is softer than nitrogen (higher value of the Fukui function), and also more negatively charged. Therefore, it would be the preferred site of electrophilic attack for both, hard and soft, electrophiles. A different situation is seen in the case of the *N*-hydroxy tautomer

where the nitrogen atom is hard (high negative charge). The lack of reactivity of this center could be attributed to the localization of the electrons lone pair in a low-lying orbital (HOMO-2).

Acknowledgment. The authors acknowledge financial support from FCE (CONICYT, Uruguay). M.B. acknowledge a fellowship granted by PEDECIBA (Uruguay). O.E.P. and E.E.C. thank CONICET (Argentina) and FAPESP (Brazil). Part of the X-ray diffraction experiments were carried out at the National Diffraction Laboratory (LANADI), La Plata, Argentina.

Supporting Information Available: Spectroscopic characterization of new compounds described in text and given in Tables 1S and 2S and Figures 1S–7S. This material is available free of charge via the Internet at <http://pubs.acs.org>.

References and Notes

- Preston, P.; Tennant, G. *Chem. Rev.* **1972**, *72*, 639.
- Smith, D. M. Benzimidazole *N*-oxides. In *Benzimidazoles and congeneric tricyclic compounds*; Preston, P. N., Ed.; John Wiley & Sons: New York, 1980; Vol. 2; p 288.
- Boiani, M.; González, M. *Mini Rev. Med. Chem.* **2004**, in press.
- Kaiya, T.; Aoyama, S.; Khoda, K. *Bioorg. Med. Chem. Lett.* **1998**, *8*, 625.
- Chua, S.; Cook, M.; Katritzky, A. *J. Chem. Soc. (B)* **1971**, 2350.
- Stacy, G. W.; Wollner, T. E.; Oakes, T. R. *Chem. Ind.* **1966**, *3*, 51.
- Ha, T. K. *Theor. Chim. Acta* **1977**, *43*, 337.
- Ochiai, E. *Aromatic amine oxides*; Elsevier: Amsterdam, 1967.
- I. Merck and Co. In *Chem. Abstr.* **1966**, *65*, 137241.
- Kamal, R.; El-Abadelah, M.; Mamad, A.; Meier, H. *Heterocycles* **1999**, *50*, 818.
- Aguirre, G.; Boiani, M.; Cerecetto, H.; Gerpe, A.; González, M.; Fernández Sainz, Y.; Ocha de Ocariz, C.; Nogál, J.; Montero, D.; Escario, J.; Denicola, A. *Arch. Pharm. (Weinheim, Ger.)* **2004**, *337*, 259.
- Desteve, G.; Brooker Brown, A.; Rose, D.; Chernov, H.; Plummer, A. J. *J. Med. Chem.* **1967**, *10*, 211.
- Gardiner, J. M.; Loyns, C. R.; Burke, A.; Khan, A.; Mahmood, N. *Bioorg. Med. Chem. Lett.* **1995**, *5*, 1251.
- Evans, T. M.; Gardiner, J. M.; Mahmood, N.; Smis, M. *Bioorg. Med. Chem. Lett.* **1997**, *7*, 409.
- Badawey, E.; Kappe, T. *Eur. J. Med. Chem.* **1999**, 663.
- Fielden, R.; Meth-Cohn, O.; Price, D.; Suschitzky, H. *Chem. Commun.* **1969**, 772.
- Enraf-Nonius. COLLECT; Nonius, B. V.: Delft, The Netherlands, 1997–2000.
- Otwinowski, Z.; Minor, W. In *Methods in Enzymology*; Carter, C. W. J.; Sweet, R. M., Eds.; Academic Press: New York, 1997; p 307.
- Sheldrick, G. M. SHELXS-97. Program for Crystal Structure Resolution; University of Göttingen: Göttingen, Germany, 1997.
- Sheldrick, G. M. SHELXS-97. Program for Crystal Structure Analysis; University of Göttingen: Göttingen, Germany, 1997.
- Spartan'04. Wavefunction, Inc.: Irvine, California.
- Halgren, T. A. *J. Comput. Chem.* **1996**, *17*, 490.
- Becke, A. D. *Phys. Rev. A* **1988**, *38*, 3098.
- Becke, A. D. *J. Chem. Phys.* **1993**, *98*, 5648.
- Lee, C.; Yang, W.; Parr, R. G. *Phys. Rev. B* **1988**, *37*, 785.
- Hay, P. J.; Wadt, W. R. *J. Chem. Phys.* **1985**, *82*, 270.
- Miertus, S.; Scrocco, E.; Tomasi, J. *Chem. Phys.* **1981**, *55*, 117.
- Barone, V.; Cossi, M.; Tomasi, J. *J. Comput. Chem.* **1998**, *19*, 404.
- Schmidt, M. W.; Baldrige, K. K.; Boatz, J. A.; Elbert, S. T.; Gordon, M. S.; Jensen, J. H.; Koseki, S.; Matsunaga, N.; Nguyen, K. A.; Su, S.; Windus, T. L.; Dupuis, M.; Montgomery, J. A. *J. Comput. Chem.* **1993**, *14*, 1347.
- <http://www.msg.ameslab.gov/GAMESS/GAMESS.html>.
- Ditchfield, R. *Mol. Phys.* **1974**, *27*, 789.
- Wolinski, K.; Hinton, J. F.; Pulay, P. *J. Am. Chem. Soc.* **1990**, *112*, 8251.
- Gauss, J. *J. Chem. Phys.* **1993**, *99*, 3629.
- Witanowski, M.; Stefaniak, L. *Bull. Pol. Acad. Sci. Chem.* **1987**, *35*, 305.
- Pfister-Guillouzo, G.; Gracian, F.; Paez, J. A.; García Gómez, C.; Elguero, J. *Spectrochim. Acta Part A* **1995**, *51*, 1801.
- Reutov, O. A.; Beletskaya, I. P.; Butin, K. P. *Carbon and Hydrogen acids (in Russian)*; Pergamon Press: Oxford, England, 1978.
- Schilf, W.; Stefaniak, L.; Webb, G. A. *Magn. Reson. Chem.* **1987**, *25*, 721.
- Martos-Calvente, R.; de la Peña O'Shea, V. A.; Campos-Martin, J. M.; Fierro, J. L. *J. Phys. Chem. A* **2003**.
- Campillo, N.; Montero, C.; Páez, J. A. *J. Mol. Struct. (THEOCHEM)* **2004**, *678*, 83.
- Johnson, C. K. ORTEP-II. A Fortran Thermal Ellipsoid Plot Program; Report ORNL 5138, Oak Ridge National Laboratory: Oak Ridge, TN, 1976.
- Peck, A. L. PLUTON, A Multipurpose Crystallographic Tool. Utrecht University: Utrecht, The Netherlands, 1988.
- Hesse, M.; Meier, H.; Zeeh, B. *Métodos Espectroscópicos en Química Orgánica*; Síntesis: Madrid, Spain, 1995.
- El-Masry, A. H.; Fahmy, H. H.; Ali Abdelwahed, S. H. *Molecules* **2000**, *5*, 1429.
- Buján de Vargas, E.; Cañas, A. I. *Tetrahedron Lett.* **1996**, *37*, 767.
- Pearson, R. J. *J. Chem. Educ.* **1987**, *64*, 561.
- Parr, R. G.; Yang, W. *J. Am. Chem. Soc.* **1984**, *106*, 4049.
- Li, Y.; Evans, J. N. S. *J. Am. Chem. Soc.* **1995**, *117*, 7756.
- Chamorro, E.; Contreras, R.; Fuentealba, P. *J. Chem. Phys.* **2000**, *113*, 10861.
- Geerlings, P.; De Proft, F.; Langenaeker, W. *Chem. Rev.* **2003**, *103*, 1793.
- Ayers, P. W.; Levy, M. *Theor. Chem. Acc.* **2000**, *103*, 353.
- Perez, P.; Simon-Manso, Y.; Aizman, A.; Fuentealba, P.; Contreras, R. *J. Am. Chem. Soc.* **2000**, *122*, 4756.
- Melin, J.; Aparicio, F.; Subramanian, V.; Galván, M.; Chattaraj, P. K. *J. Phys. Chem. A* **2004**, *108*, 2487.